

J. Electrochem. Sci. Eng. **7(4)** (2017) 153-166; DOI: <http://dx.doi.org/10.5599/jese.419>




Open Access : : ISSN 1847-9286

www.jESE-online.org

Original scientific paper

NO_x and propene conversion in La_{0.85}Sr_{0.15}MnO_{3+d}/Ce_{0.9}Gd_{0.1}O_{1.95} symmetrical cells

Anja Zarah Friedberg, Kent Kammer Hansen 

Department of Energy Conversion and Storage, Technical University of Denmark, DK-4000 Roskilde, Denmark

Corresponding authors E-mail: kkha@dtu.dk, anzf@topsoe.dk

Received: August 14, 2017; Revised: September 23, 2017; Accepted: October 10, 2017

Abstract

The catalytic electrochemical reduction of NO with propene was investigated on La_{0.85}Sr_{0.15}MnO_{3+d}/Ce_{0.9}Gd_{0.1}O_{1.95} symmetrical cells. The electrodes were infiltrated with BaO and Pt. The cells were catalytically active towards the selective catalytic reduction of NO_x with propene, but BaO infiltration lowered the NO conversion, probably because of active-site blocking on La_{0.85}Sr_{0.15}MnO_{3+d}. Pt infiltration enhanced the reduction of NO_x with propene. When a voltage was applied to the cell with BaO infiltrated electrodes, the NO conversion increased in absence and presence of propene in the feed gas and presence of 10 % O₂. The addition of propene into the feed gas did not enhance the conversion of NO when the electrodes were infiltrated with BaO. When platinum was co-infiltrated with BaO, the catalytic activity towards the reduction of NO with propene was enhanced. However, almost no effect was observed when a voltage was applied. Additionally, when the cells were infiltrated with Pt, an electrochemical promotion was observed with respect to CO₂ formation.

Keywords

NO; Propene; LSM; CGO

Introduction

Diesel engines exhibit better fuel economy than Otto engines and are thus becoming more popular. Otto engines run at a stoichiometric fuel/air ratio, whereas diesel engines operate with excess air. The exhaust contains toxic NO_x, which for engines running under a stoichiometric fuel/air ratio is efficiently removed by the so-called three-way catalytic converter (TWC). A TWC does not operate in the presence of excess oxygen; therefore, NO_x removal from a diesel engine is impossible with a TWC [1]. When removing NO_x under net oxidizing conditions, selective catalytic reduction (SCR) with ammonia/urea and NO_x storage and reduction (NSR) are the most mature technologies.

The use of SCR and NSR technologies is not straightforward. SCR technology requires on-board storage of ammonia and an ammonia slip catalyst. For the NSR technology, sophisticated engine control is needed.

In 1991, Iwamoto and Hamada [2] showed that NO_x was reduced with hydrocarbons via a process referred to as HC-SCR method. This is a potentially attractive technology because hydrocarbons already exist in exhaust gas. The HC-SCR method has been studied on precious metals such as Pt [3–5], metal oxides [6] and Ag [7,8]. It is also possible to reduce NO_x with hydrocarbons on zeolites [9–12] and perovskites [13–19]. The main issue with HC-SCR is that the activity is very low. One way to address this issue is to electrochemically promote the reduction of NO_x with hydrocarbons.

Electrochemical promotion has been well described in the literature, see *i.e.* [20]. In some cases, the rate of the enhancement in a given reaction during cell polarization is larger than that predicted by Faraday's law. This effect is referred to as the non-Faradaic electrochemical promotion of catalytic activity (NEMCA) or electrochemical promotion (EP), and is due to the back spillover of *i.e.* oxide anions to the electrodes [20]. One defines the rate enhancements factor, ρ , as

$$\rho = r/r_0 \quad (1)$$

where r is the reaction rate during polarization and r_0 is the reaction rate at OCV.

NO_x can be removed using an electrochemical reactor that is based on an oxide ion conducting electrolyte. The major drawback of the electrochemical reduction of NO_x is the simultaneous reduction of oxygen at the cathode, which leads to high power consumption. Therefore, both the activity and selectivity are important.

Jayaweera *et al.* [21] investigated the reduction of NO with CO under net oxidizing conditions. Using the perovskite La_{0.8}Sr_{0.2}Co_{0.9}Rh_{0.1}O_{3- δ} as an electrode, they showed that the reaction was electrochemically promoted under net oxidizing conditions. Earlier studies focused on metal electrodes for NO_x reduction, see [20].

The combination of a storage compound (as used in NSR technology) and electrochemical promotion appears to be an attractive solution. Traulsen *et al.* [22] investigated the use of BaO as a storage compound in an all-ceramic electrochemical cell with La_{0.85}Sr_{0.15}MnO₃/Ce_{0.9}Gd_{0.1}O_{1.95} electrodes (LSM₁₅/CGO₁₀) and found that NO could be reduced to N₂ with a conversion of 60 % at 400 °C in the presence of 10 % oxygen. Additionally, perovskites have been suggested as substitutes for Pt in NSR technology [23].

In this work, the influence of adding a reducing agent (propene) to the electrochemical reduction of NO in the presence of a storage compound BaO infiltrated in the cathode is studied. Hydrocarbons are used as reducing agents in NSR technology while an engine is running with a rich fuel/air mixture. Because Pt is normally used as a catalyst for NO oxidation in NSR technology, it is also investigated in this work.

Experimental

Symmetrical cell fabrication

For the evaluation of electrochemical cells for NO conversion with and without propene in the gas feed, symmetrical cells with LSM₁₅-CGO₁₀ electrodes, as well as with LSM₁₅-CGO₁₀ electrodes infiltrated with BaO, Pt, or BaO and Pt were used. Each of these cells consists of two identical electrodes with a dense CGO₁₀ electrolyte. LSM₁₅ powder was purchased from Haldor Topsoe A/S,

and CGO₁₀ powder was a commercial product of Rhodia. A dense 300- μ m-thick sintered tape purchased from Kerafol was used for CGO₁₀ electrolyte.

An electrode ink was prepared by mixing 50 wt% LSM₁₅ and 50 wt% CGO₁₀ powders with terpineol. The mixture was then milled on a planetary mill. Next, an ethylcellulose binder was added to the mixture, and the resulting ink was screen printed on the Kerafol electrolyte tape. The cells were then sintered at 1050 °C for 2 h and laser cut to round cells with a diameter of 13 mm. The thickness of the electrodes was approximately 15 μ m. Gold was used as the current collector, sputtered-using magnetron sputtering on top of the electrodes to generate a 50 nm porous layer. More details on the sputtering procedure can be found in [24].

The infiltration with BaO was performed using a 0.32 M aqueous solution of Ba(NO₃)₂. The solution was prepared using Ba(NO₃)₂ from Merck and Millipore water with 1 wt% P123 (BASF) as the surfactant. The cells were soaked in the solution, placed in a vacuum chamber at 0.1 mbar for 15 s and then heated to 700 °C. Pt infiltration was conducted using a 34 mM solution of Pt(NH₃)₄(NO₃)₂ (Sigma Aldrich) in Millipore water with 3 wt% of Triton-X45 (Sigma Aldrich) as the surfactant. The infiltration procedure was as previously described, and the cell was dried for several hours at 80 °C before sintering at 300 °C to decompose both the Pt complexes and surfactant. It was not possible to evaluate Pt loading because the weight of the dense electrolyte was much higher than the weight gain obtained as a result of Pt infiltration.

Test setup

Each symmetrical cell was placed in a quartz glass tube in atmospheric pressure setup, and the tube was placed inside a homemade furnace. A gas flow of 2 L/h was fed using Brooks mass flow controllers. The composition of the gas feed was 1000 ppm NO (Air Liquide; 1 % \pm 0.02 % NO in Ar) + 10 % O₂ (Air Liquide; 20 % O₂ \pm 2 % Ar) in Ar or 1000 ppm NO (Air Liquide; 1 % \pm 0.02 % NO in Ar) + 1000 ppm C₃H₆ (Air Liquide; 1 % \pm 0.02 % C₃H₆ in Ar) + 10 % O₂ (Air Liquide; 20 % O₂ \pm 2 % Ar) in Ar.

The composition of the outlet gas was monitored and recorded by a chemiluminescence detector (Model 42i HL, Thermo Scientific, USA) for NO and NO₂ detection. The propene, CO, CO₂ and N₂O concentrations were monitored using an Agilent 490 Micro Gas Chromatograph connected to the reactor and equipped with Porapak Q and Molecular Sieve 5X columns and two thermal conductivity detectors.

Microstructure and electrochemical characterization

The structure of the gold current collector layer was investigated with a HITACHI TM 3000 microscope.

A Zeiss Supra 35 scanning electron microscope was used to characterize the microstructure of the electrodes and evaluate the BaO and Pt infiltration.

A Gamry Ref 600 potentiostat-galvanostat was used for the electrochemical measurements. The Gamry was used for applying a voltage and for electrochemical impedance spectroscopy. The impedance spectra were measured in the frequency range from 878787 Hz to 1.3 mHz with 6 points per decade and amplitude of 36 mV rms.

Catalytic and electrocatalytic conversion measurements

The same testing procedure was applied for all the different cells. Each cell was placed in the setup and heated to 300 °C in air. Then, the gas feed was changed to 1000 ppm NO + 10 % O₂, and the pure catalytic conversion of NO and propene was measured.

The electrochemical measurements were conducted as follows: Before and after polarization, impedance spectroscopy measurements were performed to check whether any degradation of the cell had occurred during testing. Polarization measurements were performed for 30 min at +2 V vs. open circuit voltage (OCV). The cell was then maintained at the OCV for 30 min or until steady-state was reached, before a new test was performed. The temperature was then increased to 350 and 400 °C, and the procedure was repeated. Afterwards, the gas feed was changed to 1000 ppm NO + 1000 ppm C₃H₆ + 10 % O₂, and the electrochemical tests were repeated.

Results

Structural characterization

Representative images of the gold current collector are shown in figure 1(a) and 1(b). As shown in the figure, the current collector layer is approximately 50 nm thick and is porous as needed.

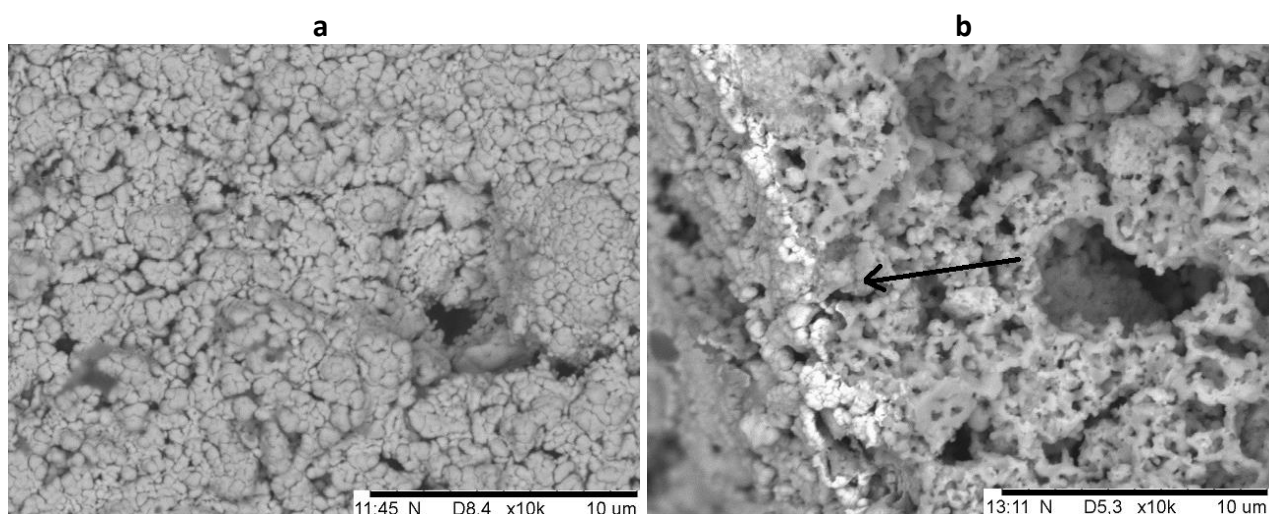


Figure 1. Microscope images of symmetrical LSM₁₅-CGO₁₀ cells: a) Gold-sputtered, porous structure. Top view; b) Gold-sputtered, thin gold layer. Side view

In figure 2(a) and 2(b), the electrode structure with BaO infiltration is shown. It is seen that before testing, the BaO nanoparticles are distributed evenly on the LSM part of the electrodes (Fig. 2(a)).

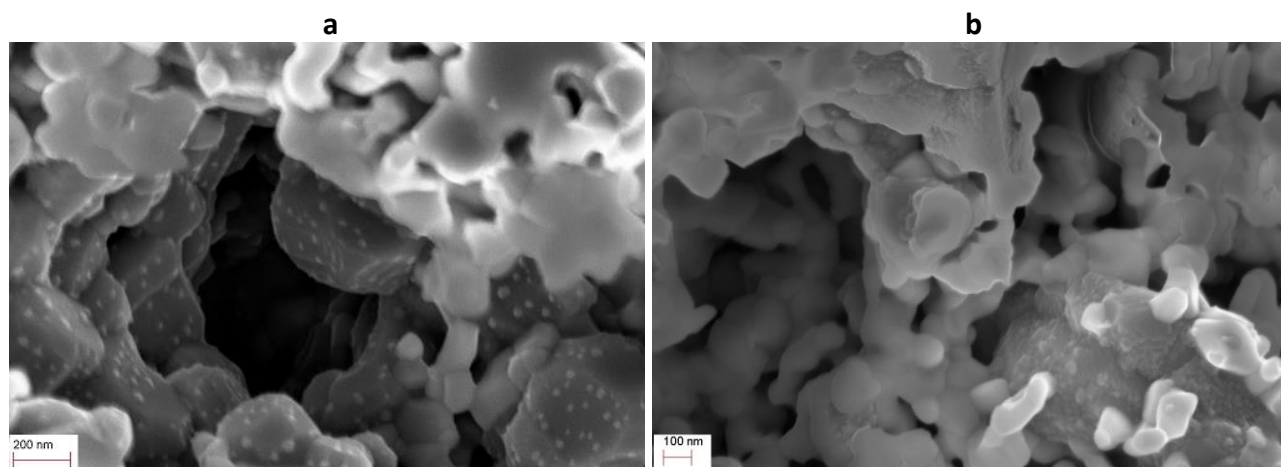


Figure 2. Microscope images of symmetrical cells with BaO infiltrated LSM₁₅-CGO₁₀ electrodes: a) before testing; b) after testing.

After testing, the BaO nanoparticle structure is fluffier, and the particles have agglomerated, which shows that BaO nanoparticles are undergoing structural changes during testing (Fig. 2(b)).

The cell electrodes infiltrated with both, BaO and Pt appeared similar to those infiltrated with just BaO. No Pt nanoparticles were observed in the SEM images. Other studies [25] have shown that the presence of Pt could not be confirmed with an EDS measurement. This result was attributed to low Pt loading and a small particle size.

Conversion measurements

All cell electrodes showed activity for the catalytic removal of NO_x. Figure 3(a) and 3(b) shows the percentage of NO_x removed in the presence and absence of propene in the gas feed. The four types of electrodes behaved very differently. At the OCV, the non-infiltrated LSM₁₅-CGO₁₀ electrodes were most active towards NO removal when propene was present, and NO conversion reached a maximum at 350 °C with a conversion degree of 8 %. When propene was absent in the gas feed, the activity decreased with increasing temperature and the NO conversion decreased to zero at 400 °C.

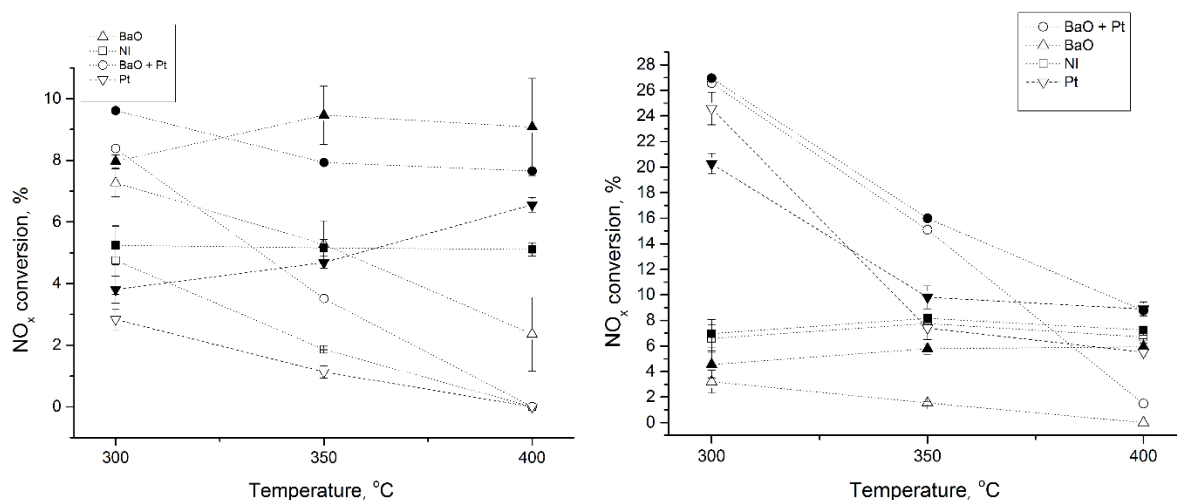


Figure 3. Percentage of NO_x conversion as a function of temperature in symmetrical cells with non-infiltrated (NI), BaO-infiltrated and BaO + Pt-infiltrated LSM₁₅-CGO₁₀ electrodes, measured at the OCV (open symbols) and during +2 V polarization (solid symbols) in: a) 1000 ppm NO + 10 % O₂; b) 1000 ppm NO + 1000 ppm C₃H₆ + 10 % O₂.

The activity of electrodes that were infiltrated with BaO decreased with increasing temperature in both atmospheres, being highest when no propene was present in the atmosphere. A conversion degree of up to 8 % was observed. The electrodes co-infiltrated with BaO and Pt revealed a higher conversion degree when propene was present. The results indicate that 27 % of NO_x was removed at 300 °C. The conversion for this cell showed highest decrease with increasing temperature. The catalytic activity of the electrodes that were infiltrated with only Pt showed activity similar to that of the non-infiltrated electrode in NO + O₂ atmosphere. In presence of propene, however, the activity increased to almost the same level as that for the BaO + Pt infiltrated electrodes. During testing in the NO + O₂ atmosphere, no N₂O was detected, and the nitrogen selectivity was 100 %. When propene was added to the gas feed, a small amount of N₂O was detected. The cells containing Pt showed the highest formation of N₂O. N₂O formation decreased with temperature as expected (N₂O is stable only at lower temperatures).

A positive effect of applying a voltage on the conversion of NO_x was observed for all types of cells under certain experimental conditions. The effect was most pronounced in the 1000 ppm NO + 10 % O₂ atmosphere (see figure 3(a) and 3(b), solid points). The selectivity to N₂ was 100 % for the non-infiltrated and Pt-infiltrated electrodes, but a small quantity of N₂O was detected for the electrodes that contained BaO. When propene was added to the feed gas, only a small polarization

effect was observed (see Table 1). The rate enhancement ratio with the polarization of the electrodes infiltrated with only BaO was highest in the presence of propene, but the extra converted NO was almost the same in both atmospheres. At 300 and 350 °C, the polarization effect on the cell with BaO + Pt infiltrated electrodes was low and less than 1 % extra NO was removed. The activity enhancement under polarization of the electrodes with only Pt and atmosphere without propene, was very similar to that of the BaO + Pt electrodes in presence of propene in gas feed, whereas it was much lower in the absence of propene. The amount of N₂O formed during polarization was the same as that at OCV. Thus, it might be argued that the NO_x converted by polarization generates N₂, whereas the NO_x that was catalytically decomposed generates N₂O.

Table 1. Rate enhancement ratio of NO_x conversion for four types of LSM15-CGO10 electrodes

	T / °C	ρ	
		Gas composition: 1000 ppm NO + 10 % O ₂	1000 ppm NO + 10 % O ₂ + 1000 ppm C ₃ H ₆
BaO	300	1.1	1.5
	350	1.9	3.8
	400	6.4	∞
BaO + Pt	300	1.1	1
	350	2.3	1
	400	15.3	6
Ni	300	1	1
	350	3	1
	400	∞	1
Pt	300	1.3	1
	350	4.3	1.3
	400	13	1.6

In figure 4(a) and 4(b), the conversions of propene and selectivity to CO₂ for the cells with BaO-infiltrated and non-infiltrated electrodes are plotted as a function of temperature.

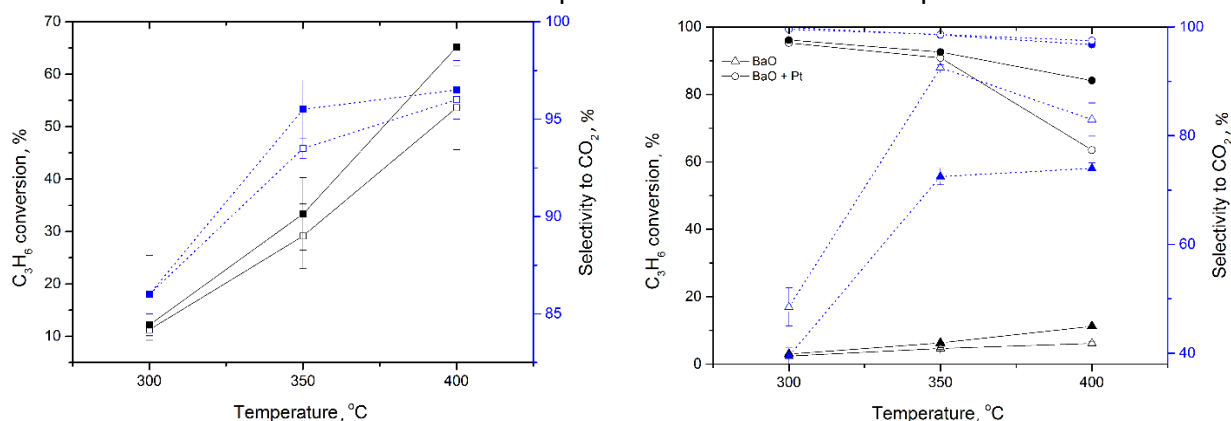


Figure 4. Temperature dependence of propene conversion (solid lines) and selectivity to CO₂ (dotted lines) in symmetrical cells measured at the OCV (open symbols) and during polarization (solid symbols) for: a) BaO and BaO + Pt-infiltrated LSM₁₅-CGO₁₀ electrodes; b) non-infiltrated LSM₁₅-CGO₁₀ electrodes.

The cells with non-infiltrated electrodes revealed a high catalytic activity, with over 60 % conversion in one of the cells at 400 °C. The cells with BaO-infiltrated electrodes showed a much lower catalytic activity towards the oxidation of propene with the highest value being just below 7 % at 400 °C. The cell with electrodes containing BaO + Pt exhibited a high catalytic conversion, where 95 % of the propene was removed at 300 °C. The conversion of propene decreased with

increasing temperature in this type of cell. The cells with only Pt infiltrated electrodes showed a 100 % conversion of propene, except at 300 °C, where only about 70 % was converted. All propene was oxidized to CO₂ since no CO was detected. For the non-infiltrated electrodes, the selectivity to CO₂ increased with increasing temperature, whereas the selectivity peaked at approximately 350 °C for the BaO-infiltrated electrodes. Almost all propene was oxidized to CO₂ in the cell with BaO + Pt electrodes at 300 and 350 °C.

The propene conversion increased to 74 % at 400 °C for the most active non-infiltrated electrodes when the cell was polarized. Additionally, when the cell was polarized, it was possible to obtain only 11 % conversion at 400 °C for the cell with BaO-infiltrated electrodes. For all the cells, the highest enhancement was obtained at 400 °C, and 84 % of the propene was removed at 400 °C in the cell with BaO + Pt infiltrated electrodes.

Electrochemical impedance spectroscopy

All impedance spectra recorded at the OCV were fitted with equivalent circuits corresponding to three and four arcs appearing in the Nyquist plots, depending on temperature and atmosphere. Most of the arcs were best fitted by an ohmic resistance model in parallel with a constant phase element (CPE). Some of the low-frequency arcs, however, could be fitted using a Voigt element, as they were almost perfect semicircles. The admittance (Y) of a CPE (denoted shortly as Q) is given by:

$$Y = Y_0 (j\omega)^n \quad (2)$$

where Y_0 is a constant, ω is the angular frequency, and n is an exponent. Y_0 and n values are estimated from the fitting of the selected equivalent circuit to the experimentally measured impedance data. The near equivalent capacitance, C_{∞} , values were estimated using the following equation:

$$C_{\infty} = (Y_0)^{1/n} R^{(1-n)/n} \quad (3)$$

The impedance spectra were fitted using Elchemea Analytical Software [26]. All impedance spectra were Kramers-Kronig validated before fitting. In the propene-containing atmosphere, the low-frequency part of the impedance spectrum obtained for the cell with BaO + Pt-infiltrated electrodes did not reach steady-state and therefore it was not possible to be fitted. Representative examples of impedance spectra and their spectral deconvolution are shown in figures 5 and 6 for the cells with non-infiltrated and BaO infiltrated electrodes measured at 400 °C.

In all Nyquist plots, two high-frequency arcs, denoted Arc I and Arc II, were observed. When propene was present in the gas feed, a small arc that could not be fitted was found in the high-frequency part of Arc I at 300 °C. Due to the high summit frequencies of Arc I (see Tables 2 and 3), part of this arc is often "dragged" down by the inductance below the real axis. This arc has an activation energy, E_a , of approximately 1 eV, and C_{∞} is independent of the atmosphere and temperature, with a value of $1 \times 10^{-7} - 9 \times 10^{-8}$ F/cm². Arc II exhibits a low n value (0.44-0.54). For the cells with the BaO-infiltrated and the non-infiltrated electrodes, C_{∞} increased with temperature. This increase was steeper for the cell with BaO-infiltrated electrodes, for which the capacitances were also higher than those for the cell with non-infiltrated electrodes. The resistance of this arc, that concerns the activation energy of the corresponding process, decreased when propene was present in the cells with non-infiltrated electrodes. No dependence on the presence of propene was observed for the resistance of this arc for the cells with BaO-infiltrated electrodes. In all impedance spectra, the dominating arc, denoted as Arc III, was observed in the middle frequency range. The activation energy of the corresponding process increased in the presence of propene for the cells

with non-infiltrated electrodes, whereas no dependence on presence of propene was observed for the cells with the BaO-infiltrated electrodes.

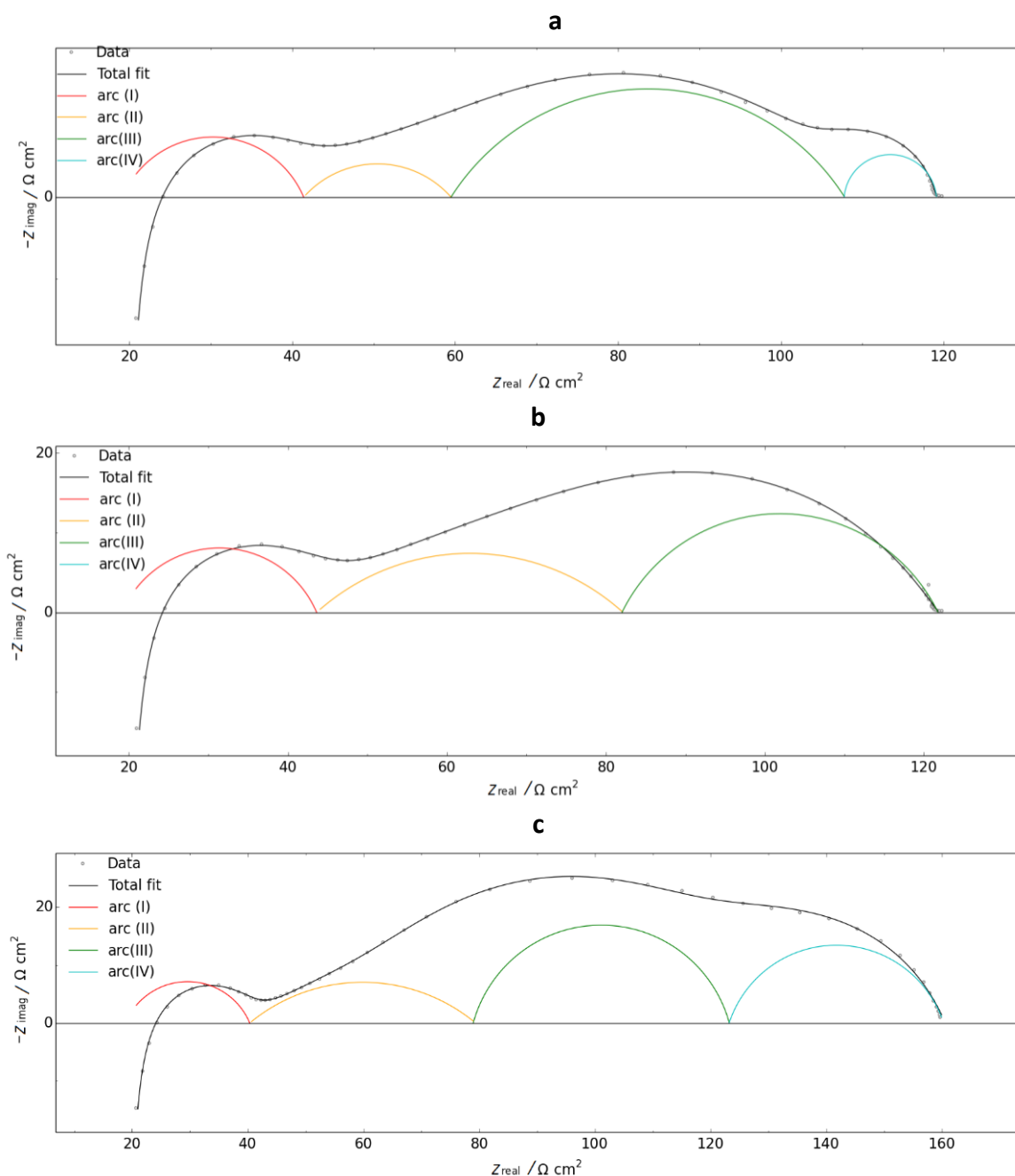


Figure 5. Nyquist plots of the impedance spectra measured at 400 °C for symmetrical cells with:
 a) non-infiltrated LSM₁₅ - CGO₁₀ electrodes in 1000 ppm NO + 10 % O₂;
 b) non-infiltrated LSM₁₅ - CGO₁₀ electrodes in 1000 ppm NO + 1000 ppm C₃H₆ + 10 % O₂;
 c) BaO-infiltrated LSM₁₅ - CGO₁₀ electrodes in 1000 ppm NO + 10 % O₂.

It was not possible to fit the high-middle to middle frequency region of the impedance spectrum of the cell with the BaO + Pt infiltrated electrodes with RQ elements having the same n (CPE) value at all three temperatures. The fitting results were not improved even after addition of more elements. The n values for Arc I and Arc IV (the low-frequency arc) were the same as for the cell with BaO infiltrated electrodes, but the n values of Arc II and Arc III changed with temperature. Therefore, no activation energies or capacitance values could be calculated for Arc II and Arc III for this cell. Instead, the total resistance of these two arcs was used to obtain activation energies of

0.91 eV and 0.97 eV in the presence and absence of propene, respectively. A low-frequency arc (Arc IV) with a high n value was observed in the impedance spectra of all cells. This arc appeared only in the NO + O₂ atmosphere for the cell with non-infiltrated electrodes, but in the cells with BaO infiltrated electrodes, the arc was observed in both types of gas mixture. This arc was not observed at 300 °C. In all cases, the n value of the CPE was the highest at 350 °C. For the cell with non-infiltrated electrodes, the change in n value with increasing temperature was small, with n decreasing from 0.97 to 0.92. However, the n value was higher for the cell with BaO infiltrated electrodes, especially in the presence of propene, where it decreased from 1 to 0.6. The behavior was the same in the BaO + Pt cells. The resistance corresponding to this arc was changed by only a small amount with increasing temperature.

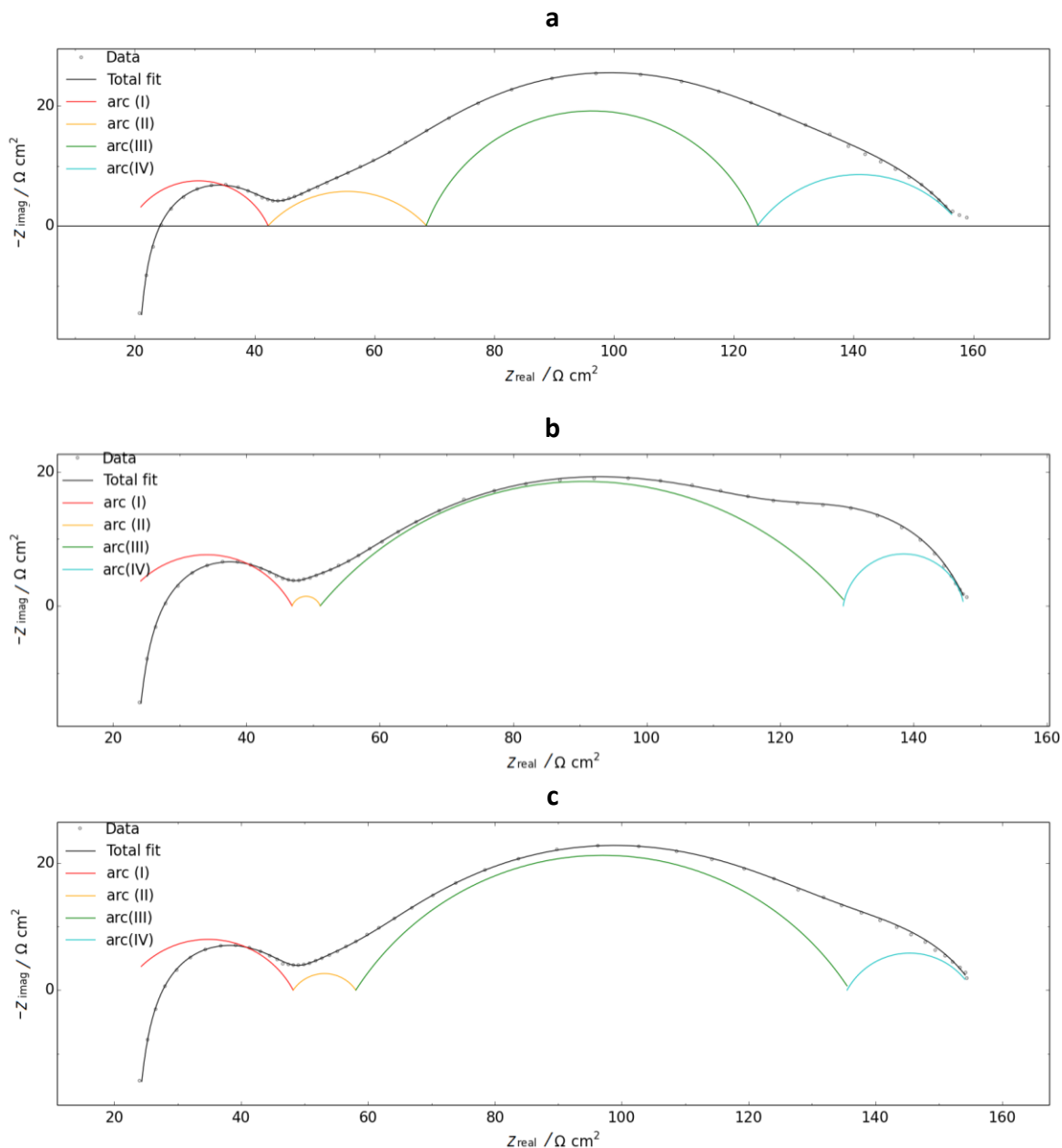


Figure 6. Nyquist plots of the impedance spectra measured at 400 °C for symmetrical cells with:
 a) BaO-infiltrated LSM₁₅- CGO₁₀ electrodes in 1000 ppm NO + 1000 ppm C₃H₆ + 10 % O₂;
 b) BaO + Pt-infiltrated LSM₁₅- CGO₁₀ electrodes in 1000 ppm NO + 10 % O₂;
 c) BaO + Pt-infiltrated LSM₁₅- CGO₁₀ electrodes in 1000 ppm NO + 1000 ppm C₃H₆ + 10 % O₂.

Table 2. Characteristics of the processes corresponding to different arcs of the impedance spectra of the symmetrical cell with non-infiltrated LSM₁₅-CGO₁₀ electrodes, measured at 300-400 °C in the atmosphere containing 1000 ppm NO +10 % O₂

Processes/Arcs	$f_{\text{summit}} / \text{Hz}$	$C_{\text{w}} / \text{F cm}^{-2}$	Characteristics
I	$4 \times 10^3 - 9 \times 10^5$	$\sim 10^{-7}$ Independent of temperature and atmosphere.	$E_a = 0.9 \pm 0.06 \text{ eV}$ Independent of atmosphere.
II	17-661	$4 \times 10^{-6} - 3.5 \times 10^{-5}$ Increased with increasing temperature. Higher values in the presence of propene.	$E_a = 0.75-1 \text{ eV}$ Decreases when propene is present. Resistance decreases with polarization. f_{summit} values are higher when propene is present. $n = 0.44 - 0.54$
III	0.5-19	$1.6 \times 10^{-4} - 6 \times 10^4$ Independent of temperature. Higher values in the presence of propene.	$E_a = 0.71-0.92 \text{ eV}$ Increases when propene is present. f_{summit} values are independent of atmosphere.
IV			High n value ($n = 1$) Appears at 350 and 400 °C at OCV in NO + O ₂ . Appears in the presence and absence of propene. Resistance is independent of temperature.

Table 3. Characteristics of the processes corresponding to different arcs of the impedance spectra of the symmetrical cell with BaO-infiltrated LSM₁₅-CGO₁₀ electrodes, measured at 300-400 °C in the atmosphere containing 1000 ppm NO + 1000 ppm C₃H₆ + 10 % O₂.

Processes/Arcs	$f_{\text{summit}} / \text{Hz}$	$C_{\text{w}} / \text{F cm}^{-2}$	Characteristics
I*	3000-90000	$\sim 10^{-7}$ Independent of temperature and atmosphere.	$E_a = 0.94 \pm 0.02 \text{ eV}$
II	3-65	$5.4 \times 10^{-5} - 2 \times 10^{-4}$ Increased with increasing Temperature. Higher values in absence of propene.	$E_a \sim 0.95 \pm 0.1 \text{ eV}$ f_{summit} is higher when propene is present. $n = 0.44 - 0.54$
III	0.2-2	$9 \times 10^{-4} - 1.6 \times 10^4$ Increased with higher temperatures. Higher values in presence of propene.	$E_a = 0.81-0.93 \text{ eV}$ Increases when propene is present f_{summit} are independent of atmosphere.
IV*	0.012-0.1		Appears at 350 and 400 °C at the OCV $n = 0.6$

* including results for the BaO + Pt infiltrated electrode

Discussion

Conversion and the effect of propene

When a voltage was applied to the cells with BaO infiltrated electrodes, the NO_x conversion increased. The enhancement factor, ρ , was highest in a propene atmosphere, but the amount of N₂ formed was almost the same in the presence and absence of propene. A higher ρ observed in the propene-containing atmosphere can be attributed to the lower catalytic activity in this case. The lower catalytic activity in the propene-containing atmosphere suggests that the reduction of NO was inhibited by propene when BaO is used as a storage compound. However, the catalytic activity

of the non-infiltrated electrodes was promoted in the presence of propene, which supports the findings of Hansen *et al.* [13], who found that LSM is a catalyst for the SCR of NO with propene. It is well known that NO₂ is an intermediate in the reduction of NO to nitrogen when using a storage compound. Propene and NO will then compete for the same active sites on LSM. When propene is present, fewer active sites are available for NO oxidation, and BaO will cover some of the active sites on LSM. This coverage could be the reason for the lower activity of BaO infiltrated electrodes in the presence of propene. The catalytic reduction of NO on the BaO + Pt infiltrated electrodes showed a dependence on temperature similar to the other tested electrodes, but NO_x conversion was much higher and much more dependent on temperature. For the cells with electrodes infiltrated with Pt and BaO, the higher conversion in the NO + O₂ atmosphere could be attributed to both, the removal via a storage compound and Pt. In the presence of propene, the higher conversion in this cell at high temperatures could be attributed to the excellent oxidation ability of the Pt catalyst. The positive effect of polarization in the propene-containing atmosphere was highest for the cell with BaO-infiltrated electrodes at all three temperatures. However, the total NO_x conversion was low for this type of the cell but equally high as that for the cell with the BaO + Pt infiltrated electrodes when propene is present. The presence of platinum together with BaO in electrodes provided a higher NO conversion in the presence of propene at 300 and 350 °C, compared to electrodes with either Pt or BaO. This finding may indicate that Pt enhances nitrate formation by forming NO₂, which is the step preceding nitrate formation [27]. The higher conversion could also be simply attributed to the sum of the reactions via BaO and Pt. The amount of N₂O found for the cell with the BaO + Pt infiltrated electrodes was much higher than that formed in the cells with electrodes infiltrated only with BaO, where almost nothing was formed when propene was present. The amount of N₂O formed in the cell with BaO + Pt infiltrated electrodes was similar, but still higher than that formed in the cell with electrodes infiltrated only with Pt. The reduction route via the storage compound is still not known for certain [28], but formation of N₂O could suggest that the production from nitrate occurs via Pt, which simply reduces it only to N₂O in the presence of propene. The total conversion of NO_x in the presence of propene was higher on the non-infiltrated electrodes than in BaO infiltrated ones. The reduction of NO could occur via different routes, depending on the nature of the catalyst. The LSM behaved as a catalyst for the SCR of NO with propene, and this reaction was not significantly enhanced by polarization. In the cells with BaO-infiltrated electrodes, the reduction could also proceed via nitrate formation. The formation of N₂ in the presence and absence of propene suggests that nitrate formation was not coupled with propene oxidation. On the Pt containing electrodes, the reduction could proceed via LSM or Pt. In the presence of propene, polarization decreased NO_x conversion on the Pt containing electrodes. This effect might be explained by the behavior of NO_x reduction on Pt, which is known to peak as a function of temperature. This peak occurs at a lower temperature upon polarization [29], which means that if one is looking at only three temperatures, the peak could easily be missed, and the observed behavior can look like if the polarization has a negative effect.

Impedance analysis

The polarization resistance of the cells with non-infiltrated electrodes is similar for the two tested cells, which indicates good reproducibility. In all impedance spectra obtained at 300 °C in the propene-containing gas, a small arc in the high-frequency range was observed. It was not possible to fit the arc, but it was clear that it overlapped with the larger high-frequency arc, referred as Arc I.

Clearly, something occurred in the presence of propene in the atmosphere, which caused this response at high frequencies. At this point, it is not possible to determine the origin of this arc.

The change in the activation energy corresponding to the resistance of the high-frequency arc (Arc I) with the addition of propene can be explained by the presence of this small high-frequency arc. The capacitance and summit frequencies together with an E_a close to 1 eV indicate that oxide ion transport across the interface of the electrode and electrolyte is responsible for this impedance response [30-32].

The near-equivalent capacitance of Arc II was higher in the cells containing BaO infiltrated electrodes. In these cells, the value of C_{∞} decreased when propene was introduced in the atmosphere. The opposite was observed for the cells with non-infiltrated electrodes, in which the presence of propene increased the capacitance. The higher value of C_{∞} for the cell with BaO-infiltrated electrodes can be associated with the presence of BaO and better adsorption of NO on BaO sites compared to LSM sites.

The capacitance value of the Arc II was close to capacitance values associated with oxygen adsorption and dissociation on the composite electrode [22]. The higher capacitance of the cells with BaO-infiltrated electrodes could be related to the production of active oxygen species by reduction of nitrates. The decrease in C_{∞} observed when propene is present in the cell with BaO-infiltrated electrodes could indicate that propene interacts via the above mentioned reaction, which is supported by a decrease in NO reduction in the presence of propene. In the cells with non-infiltrated electrodes, propene could interact with adsorbed oxygen, thereby forming more active oxygen species for dissociation on the electrode surface. The near-equivalent capacitance correlated well with the capacitance values related to oxygen adsorption and dissociation on the electrode surface reported in earlier findings from our group [22,33].

In the case of Arc II, the C_{∞} value of the MF arc (Arc III) observed for the cells with BaO infiltrated electrodes was higher than that for non-infiltrated electrodes. The increase of C_{∞} and decrease of the resistance of this arc with increasing temperature indicates that the responsible process is related to the extension or broadening of the three-phase boundary [34]. The E_a corresponding to this process increased for both cells with the non-infiltrated and BaO-infiltrated electrodes, when propene was introduced in the gas feed. The values of E_a are in good agreement with previous findings of our group [33,35], where the processes related to the corresponding arc were stated as adsorption, surface diffusion and transfer across the triple-phase boundary (TPB). The sensitivity of E_a in the presence of propene was reasonable since different species will adsorb in two atmospheres, while propene is believed to interact with adsorbed oxygen [34]. For these reasons, the Arc III is ascribed to the triple-phase boundary that is related to adsorption, diffusion and/or charge transfer involving oxygen and nitric oxide species.

The change in the n values for Arc II and Arc III observed for the cell with BaO + Pt infiltrated electrodes suggests that these arcs represent different processes at different temperatures. In this cell, propene conversion decreased with increasing temperature, opposite to what is expected for a platinum catalyst [29]. This result suggests that something changes in the structure of the cell that inhibited this oxidation reaction. One explanation could be that the BaO nanoparticles which created a fluffier structure after testing covered the platinum nanoparticles, thereby inhibiting the reaction by lowering the number of active sites. This change in microstructure could also lead to a change in the impedance response. Arcs II and III were related to the adsorption, dissociation, and diffusion of surface species at BaO infiltrated and non-infiltrated electrodes. These processes were very dependent on the infiltrated materials.

Adsorption on BaO is believed to proceed through NO₂ [22], whereas the chemisorption of NO is expected on Pt [29,36]. This means that when both, Pt and BaO nanoparticles are present, the adsorption and reduction of NO can proceed via different pathways. The impedance response, shown as Arc II and Arc III, might correspond to a mixture of these processes.

In some of the impedance spectra, a low-frequency arc was found, but not for the cells with non-infiltrated electrodes in the presence of propene. The size of this arc and the n value were difficult to be determined from the impedance spectra measured at the OCV. In view of the low activation energy related to this arc, the fact that it appears at low frequencies of impedance spectra of all cells regardless of impregnation material, is in good agreement with the gas diffusion impedance, as described by Mogensen [37].

In both cells with BaO and BaO + Pt infiltrated electrodes, the low-frequency parts of impedance spectra changed at 350 °C and 400 °C. The n value of the low-frequency arc was found to be approximately 0.9 in the absence of propene, but it decreased to approximately 0.7 in the presence of propene at 400 °C. It was not possible to create a better fit with additional arcs. The different n values of the arcs could represent two different processes at two different temperatures in the presence of propene in the gas phase.

Conclusions

In this work, it was shown that the catalytic reduction of NO by propene on La_{0.85}Sr_{0.15}MnO₃/Ce_{0.9}Gd_{0.1}O_{1.95} (LSM₁₅/CGO₁₀) electrodes in the presence of excess of oxygen was not electrochemically enhanced. However, the direct reduction of NO was enhanced in the presence of excess oxygen. The impregnation of LSM₁₅/CGO₁₀ with BaO increased the removal of NO, and an electrochemical enhancement was observed in the absence and presence of propene in the gas feed. No coupling between the oxidation of propene and reduction of NO via BaO was observed. Propene oxidation was inhibited by the presence of BaO nanoparticles on the LSM₁₅/CGO₁₀ surface because they covered the active sites for propene oxidation. The impregnation of LSM₁₅/CGO₁₀ with Pt significantly enhanced the HC-SCR, but only a minor electrochemical promotion of this reaction was achieved.

References

- [1] N. Guillen-Hurtado, V. Rico-Perez, A. Garcia-Garcia, D. Lozano-Castello, A. Bueno-Lopez, *DYNA* **79** (2012) 114-121
- [2] M. Iwamoto, H. Hamada, *Catalysis Today* **10** (1991) 57-71
- [3] R. Burch, J.P. Breen, F.C. Meunier, *Applied Catalysis B: Environmental* **39** (2002) 283-303
- [4] A. Iglesias-Juez, A.B. Hungria, A. Martinez-Arias, A. Fuerte, M. Fernandez-Garcia, J.A. Anderson, J.C. Conesa, J. Soria, *Journal of Catalysis* **217** (2003) 310-323.
- [5] A. Obuchi, A. Ohi, M. Nakamura, A. Ogata, K. Mizuno, H. Ohuchi, *Applied Catalysis B: Environmental* **2** (1993) 71-80.
- [6] H. Hamada, *Catalysis Today* **22** (1994) 21-40.
- [7] E. F. Iliopoulou, A. P. Evdou, A. A. Lemonidou, I. A. Vasalos, *Applied Catalysis A: General* **274** (2004) 179-189.
- [8] H. Kannisto, H. Ingelsten, M. Skoglundh, *Journal of Molecular Catalysis A: Chemical* **302** (2009) 86-96
- [9] M. Sasaki, H. Hamada, Y. Kintaichi, T. Ito, *Catalysis Letter* **15** (1992) 297-304.
- [10] H. Hamada, Y. Kintaichi, M. Sasaki, T. Ito, M. Tabata, *Applied Catalysis* **70** (1991) L15-L20.
- [11] G. P. Ansell, A. F. Diwell, S. E. Golunski, J. W. Hayes, R. R. Rajaram, T. J. Truex, A. P. Walker, *Applied Catalysis B: Environmental*, **2** (1993) 81-100.
- [12] K. A. Headon, D. K. Zhang, *Industrial & Engineering Chemistry Research*, **36** (1997) 4595-4599.
- [13] K. K. Hansen, E. M. Skou, H. Christensen, T. Turek, *Journal of Catalysis* **199** (2001) 132-140.

- [14] X. Wu, L. Xu, D. Weng, *Catalysis Today* **90** (2004) 199-206.
- [15] F. C. Buciuman, E. Joubert, J. Barbier, J. C. Menezes, *Applied Catalysis B: Environmental* **35** (2001) 149-156.
- [16] R. Zhang, A. Villanueva, H. Alamdari, S. Kaliaguine, *Applied Catalysis A: General* **307** (2006) 85-97.
- [17] J. Lentmaier, S. Kemmler-Sack, G. Knell, P. Kessler, E. Plies, *Material Research Bulletin* **31** (1996) 1269-1976.
- [18] V. N. Stathopoulos, V. C. Belessi, T. V. Bakas, S. G. Neophytides, C. N. Costa, P. J. Pomonis, A. M. Efstathiou, *Applied Catalysis B: Environmental* **93** (2009) 1-11.
- [19] J.C. Menezes, S. Inkari, T. Bertin, J. Barbier, N. Davias-Bainier, R. Noirot, T. Seguelong, *Applied Catalysis B: Environmental* **15** (1998) L1-L4.
- [20] C.G. Vayenas, S. Bebelis, C. Pliangos, S. Brosa, D. Tsiplakides, *Electrochemical Activation of Catalysis: Promotion, Electrochemical Promotion, and Metal-Support Interactions*, Kluwer Academic/Plenum Publishers, New York (2001).
- [21] P. Jayaweera, A. Sanjurjo, G. Krishnan, E. D. Wachsman, *Solid State Ionics* **136** (2000) 775-782.
- [22] M. L. Traulsen, K. B. Andersen, K. K. Hansen, *Journal of Materials Chemistry* **22** (2012) 11792-11800.
- [23] C. Hwan Kim, G. Qi, K. Dahlberg, W. Li, *Science*, **327**(5973) (2010) 1624-1627
- [24] H. Abdul, J., Mohammed, J. V. T. Høgh, W. Zhang, E. Stamate, K. Thydén, N. Bonanos, *Journal of Power Sources* **212** (2012) 247-253.
- [25] J. Shao, *Low Temperature NO_x decomposition using an electrochemical reactor*, Ph.D. Thesis, DTU Energy Conversion, (2013)
- [26] Elechemea analytical. <http://www.elchemea.com>, 2012. Accessed: 2014-07-08.
- [27] S. Matsumoto, *CATTECH* **4** (2000) 102-109.
- [28] G. Liu, P. Gao. *Catalysis Science & Technology* **1** (2011) 552-568.
- [29] B. Beguin, F. Gaillard, M. Primet, P. Vernoux, L. Bultel, M. Henault, C. Roux, E. Siebert, *Ionics* **8** (2002) 128-135.
- [30] M. J. Jorgensen, M. Mogensen, *Journal of Electrochemical Society* **148** (2001) A433-A442.
- [31] M. L. Traulsen, K. K. Hansen, *Journal of Electrochemical Society* **158** (2011) P147-P161.
- [32] D. Ippolito, K. B. Andersen, K. K. Hansen, *Journal of Electrochemical Society* **159** (2012) P57.
- [33] J. Shao, K. K. Hansen, *Journal of Electrochemical Society* **160** (2013) H494-H501.
- [34] D. Ippolito, K. K. Hansen, *Journal of Solid State Electrochemistry* **17** (2013) 895-908.
- [35] R. M. L. Werchmeister, K. K. Hansen, M. Mogensen, *Journal of Electrochemical Society* **157** (2010) P107-P112.
- [36] M. Konsolakis, I. V. Yentekakis, *Journal of Hazardous Materials* **149** (2007) 619-624.
- [37] S. Primdahl, M. Mogensen, *Journal of Electrochemical Society* **146** (1999) 2827-2833.